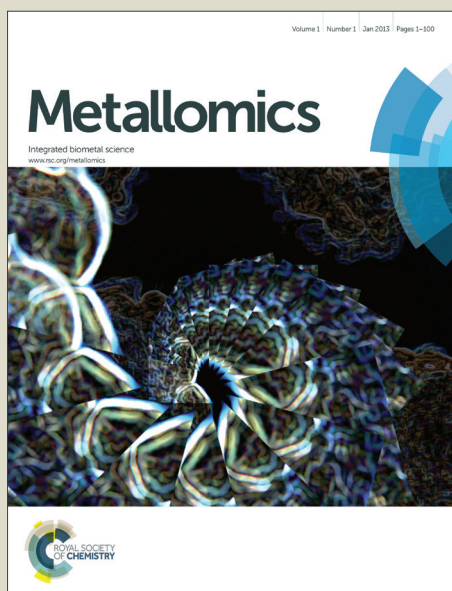This is an *Accepted Manuscript*, which has been through the Royal Society of Chemistry peer review process and has been accepted for publication.

Accepted Manuscripts are published online shortly after acceptance, before technical editing, formatting and proof reading. Using this free service, authors can make their results available to the community, in citable form, before we publish the edited article. We will replace this *Accepted Manuscript* with the edited and formatted *Advance Article* as soon as it is available.

You can find more information about *Accepted Manuscripts* in the **Information for Authors**.

Journal Name

ARTICLE

Discovery of A Dual-Targeting Organometallic Ruthenium Complex With High Activity Inducing Early Stage Apoptosis of Cancer Cells

Jun Du,[a] Erlong Zhang,[a, b] Yao Zhao,[b*] Wei Zheng,[b] Yang Zhang,[b] Yu Lin,[b] Zhaoying Wang,[b] Qun Luo,[b] Kui Wu,[b] Fuyi Wang[b*]

Abstract: Ruthenium based complexes are promising antitumour candidates due to their lower toxicity and better water-solubility compared to the platinum antitumour complexes. Epidermal growth factor receptor (EGFR) has been found to be overexpressed in a large set of tumour cells. In this work, a series of organoruthenium complexes containing EGFR-inhibiting 4-anilinoquinazoline pharmacophores were synthesised and characterised. These complexes were shown excellent inhibitory activity against EGFR and high affinity to interact with DNA via minor groove binding, featuring dual-targeting property. In vitro screening demonstrated that the as-prepared ruthenium complexes are anti-proliferating towards a series of cancer cell lines, in particular the non-small-cell lung cancer cell line A549. Fluorescence-activated cell sorting analysis and fluorescence microscopy revealed that the most active complex **3** induced much more early-stage cell apoptosis than its cytotoxic arene ruthenium analogue and the EGFR-inhibiting 4-anilinoquinazolines, verifying the synergetic effect of the two mono-functional pharmacophores.

Introduction

Cancer is a severe and still growing threat to human health. Since the first discovery of cisplatin as an effective antitumour agent in late 1960s, various platinum analogues have been extensively studied and some of them have been successfully used in clinic such as carboplatin and oxaliplatin.[1] However, the administration of cisplatin and its analogues in clinic is limited by their poor water solubility, severe dose-limiting side effects such as nephrotoxicity, neurotoxicity and myelosuppression, and inherent or acquired resistance.[2, 3] In recent years, other metal-based antitumour agents such as ruthenium, osmium, and iridium, have shown promising anticancer effects, providing good alternative to platinum-based drugs.[4-11]

[a] College of Chemistry and Materials Science, Key Laboratory of Functional Molecular Solids, The Ministry of Education, Anhui Laboratory of Molecular-Based Materials, Anhui Normal University, Wuhu 241000, P. R. China.

[b] Beijing National Laboratory for Molecular Sciences; CAS Key Laboratory of Analytical Chemistry for Living Biosystems; Beijing Centre for Mass Spectrometry; Institute of Chemistry, Chinese Academy of Sciences, Beijing 100190, P. R. China. Email: fuyi.wang@iccas.ac.cn; yaozhao@iccas.ac.cn

Among the large library of non-platinum antitumour complexes, ruthenium based complexes have attracted increasing interest due to their high efficacy, good water solubility and low toxicity.[8-19] Two Ru[III] complexes, NAMI-A and KP1019 are now under phase II clinical trials,[20, 21] and the organometallic half-sandwich ruthenium(II) complexes in type of $[(\eta^6\text{-arene})Ru(X)(Y)(Z)]$ have been extensively studied in recent years.[22-26] This kind of complexes adopt an octahedral geometry, of which three coordination sites are occupied by arene ligands, stabilizing the ruthenium centre in +2 oxidative status, and other three sites offer possibilities for coordination with a variety of ligands to tune their biological activities, such as hydrophobicity, cellular uptake, reactivity and selectivity towards biological targets.[6-8, 27] For instance, the $\{(\eta^6\text{-arene})Ru\}$ (arene = cyclopentadienyl, benzene, *p*-cymene, biphenyl, etc.) units can coordinate with ethylenediamine, imidazole, 2-(aminomethyl)pyridine, derived enzyme inhibitors to get a series of novel complexes with diverse biological activity and improved antitumour activity,[24, 28-33] indicating the possibility of organometallic ruthenium(II) arene complexes for the development of multi-functional antitumour drugs.

The epidermal growth factor receptor (EGFR), which belongs to receptor tyrosine kinase (RTK) family, plays an important role in the cellular signal transduction and thus regulates cell growth. EGFR is overexpressed in a broad type of

human cancer cells such as squamous carcinoma, cervical cancer, lung cancer cells,[34] which make it an attractive target for developing novel antitumour drugs. It was found that blocking the ATP binding site of EGFR can inhibit its tyrosine kinase activity, so as to inhibit the growth of tumours.[35] In light of this discovery, many kinds of ATP-competitive EGFR inhibitors have been developed as antitumour agents. To date, 4-anilinoquinazoline derivatives have shown good potency in inhibiting EGFR and EGF-stimulated growth of a certain type of cancer cells. Some of them, for instance, gefitinib and erlotinib, have been widely used in clinic for the therapy of non-small-cell lung cancer and squamous carcinoma.[34] Compared to the traditional cytotoxic antitumour drugs, this kind of drugs has much less toxicity towards normal tissues while being high active against tumour tissues, and is described as "Molecular Targeting Drugs".[36, 37]

Since cancer is a multigenic disease, the drugs that can act on two or more targets may achieve better therapeutic effect than the mono-functional drugs. In the previous works of our group, we utilized the "pharmacophore conjugation" strategy to design and synthesise a series of dual-functional ruthenium antitumour complexes. We modified the 6-position of 4-anilinoquinazoline pharmacophore with either ethylenediamine or imidazole so that the modified anilinoquinazolines could be coordinated to Ru^{II} or Ru^{III} to give a series of novel ruthenium complexes. An important character of these complexes is that there are two different pharmacophores in one molecule: one is the $\{(arene)Ru^{II}\}$ group[30] or the $\{Ru^{III}Cl_n(DMSO)_m]\}$ fragment[38] which is likely responsible for inducing DNA damage; the other one is the 4-anilinoquinazoline group which acts as the EGFR inhibitor. Those two pharmacophores endue the ruthenium complexes dual-targeting property. Among them, a Ru^{III} complex and a Ru^{II} complex, of which both contain the 4-anilinoquinazoline ligand 6-(2-(2-aminoethylamino)ethoxy)-4-(3'-chloro-4'-fluoroanilino)-7-methoxy-quinazoline (L0), exhibited excellent and selective antiproliferative activity towards the EGF (epidermal growth factor) stimulated growth of human MCF-7 breast cancer with better ability inducing apoptosis than the mono-functional EGFR-inhibiting gefitinib.[30, 38] However, the complex [$Ru^{III}Cl_4(DMSO)(L3)$] (L3 = 6-(2-(2-(1H-imidazol-1-yl))ethoxy)-4-(3'-chloro-4'-fluoroanilino)-7-methoxy-quinazoline, Scheme 1) exhibited little cytotoxicity towards MCF-7 cancer cell line (IC$_{50}$ > 100 μM), though it is more active against the enzyme activity of EGFR than the complex [$Ru^{III}Cl_3(DMSO)(L0)$].[38] Since Ru^{II} arene complexes usually possess higher cytotoxicity than Ru^{III} complexes,[39] in order to improve the antitumour activity of Ru-L3 complexes, in this work, two complexes, [(η^6-p-cymene)Ru^{II}(L3)Cl$_2$] (3) and [(η^6-p-cymene)Ru^{II}(en)L3]$^{2+}$ (4) were prepared. In addition, to examine the structure activity relationships of this kind of dual targeting antitumour agents and thus further explore the mechanisms of their antitumour activity, three analogues were also prepared (complexes 1, 2, and 5) using imidazole and 2-(aminomethyl)pyridine as the coordination ligands to $\{(p$-cymene)$Ru^{II}\}$ fragment. These complexes were synthesised and characterised by NMR, MS

and elemental analysis, and complex 4 was further characterised with X-ray crystallography analysis. Their biological activities have been evaluated using enzyme-linked immunosorbent assay (ELISA), anti-proliferation assay and molecular modelling analysis.

Experimental Section

Materials

The staring material 6-hydroxy-4-(3'-chloro-4'-fluoroanilino)-7-methoxy-quinazoline was purchased from Shanghai FWD Chemical Co, [(η^6-p-cymene)RuCl$_2$]$_2$ from TCI (Shanghai) Development Co., Ltd. (China), 1, 2-dibromoethane and 1, 3-dibromopropane from Beijing Ouhe Technology Co. (China), ethylenediamine from Beijing Xingjin Chemicals Co. (China). Organic solvents including absolute methanol, absolute ethanol, absolute ether, acetonitrile, dichloromethane and DMSO were all analytical grade and used directly without further purification. Column chromatography silica gel and thin layer chromatography silica gel were purchased from Qingdao Jiyida Silica Reagent Manufacture (China). All ^{1}H NMR and ^{13}C NMR were recorded on an Avance III 400 spectrometer (Bruker).

Synthesis of 6-(2-(2-(pyridin-2-yl-methylamino))ethoxy)-4-(3'-chloro-4'-fluoroanilino)-7-methoxy-quinazoline (L1)

6-hydroxy-4-(3'-chloro-4'-fluoroanilino)-7-methoxy-quinazoline (319 mg, 1 mmol) and potassium carbonate (552 mg, 4 mmol) were added to DMF (30 mL) and stirred at ambient temperature for 0.5 h. Then 1, 2-dibromoethane (0.34 mL, 4 mmol) was added and the resulting mixture was heated at 80 °C for 4 h. After cooling to room temperature, the solid was filtered off. The filtrate was concentrated to 3 mL in vacuum, and the resulting residue was purified by flash chromatography on Silica gel using ethyl acetate/petroleum (5:3) as eluent giving L′1 as white powder (254 mg, 60%). Then 6-(2-(2-bromoethoxy)ethoxy)-4-(3'-chloro-4'-fluoroanilino)-7-methoxy-quinazoline (L′1) (424 mg, 1 mmol) and 2-(aminomethyl)pyridine (393 μL, 4 mmol) were added to DMF (10 mL) and the mixture was heated at 80 °C for 4 h. After concentrating, cooling to room temperature, the mixture was poured into water (40 mL), and the forming precipitate was collected by centrifugation, purified by flash chromatography on silica gel using chloroform/methanol (20:1) as eluent giving 6-(2-(2-(pyridin-2-yl-methylamino))ethoxy)-4-(3'-chloro-4'-fluoroanilino)-7-methoxy-quinazoline (L1) as yellow powder (272 mg, 60%). ESI-MS (m/z): 454.146 ([M + H]$^+$, C$_{23}$H$_{22}$N$_5$O$_2$ClF requires 454.141); m. p. 93 – 96 °C. ^{1}H NMR (DMSO-d_6, 400 MHz) δ (ppm): 8.51 (s, 2H); 8.14 (dd, 1H); 7.85 (s, 1H); 7.84 – 7.80 (m, 1H); 7.76 (td, 1H); 7.49 – 7.42 (m, 2H); 7.25 (dd, 1H); 7.21 (s, 1H); 4.25 (t, 2H); 3.95 (s, 3H) 3.93 (s, 2H); 3.04 (t, 2H). Anal. calcd. (%) for C$_{23}$H$_{21}$ClFN$_5$O$_2$: C, 60.86; H, 4.66; N, 15.43; Found: C, 60.44; H, 4.64; N, 15.78.

Synthesis of 6-(2-(3-(pyridin-2-yl-methylamino))propoxy)-4-(3'-chloro-4'-fluoroanilino)-7-methoxy-quinazoline (L2)

4-(3'-chloro-4'-fluoroanilino)-6-hydroxy-7-methoxy-quinazoline (319 mg, 1 mmol) and potassium carbonate (552 mg, 4 mmol) were added in acetone (60 mL) and stirred at ambient temperature for 0.5 h. Then 1, 3-dibromopropane (0.34 mL, 4 mmol) was added and the resulting mixture was heated at 70 °C for 7 h. Then cooling to room temperature, The solid was filtered off, and after concentrating, the residue was chromatographed by flush chromatography on Silica gel using ethyl acetate/petroleum (5:3) as eluent to give L'2 as yellow powder (284.7 mg, 65%). Then we used 6-(2-(3-bromoethoxy)propoxy)-4-(3'-chloro-4'-fluoroanilino)-7-methoxy-quinazoline (L'2) (438 mg, 1 mmol) and 2-(aminomethyl)pyridine (393 μL, 4 mmol) were added in DMF (10 mL) and the resulting mixture was heated at 80 °C for 4 h. After concentrating solution, cooled to room temperature, the mixture was poured into water (40 mL), the obtained deposit was got by centrifugation, and the residue was chromatographed by using column chromatography on silica gel using chloroform/methanol (20:1) as eluent to give 6-(2-(3-(pyridin-2-yl-methylamino))propoxy)-4-(3'-chloro-4'-fluoroanilino)-7-methoxy-quinazoline (L2) as yellow powder (269 mg, 60%). ESI-MS (m/z): 468.161 ([M + H]$^+$, $C_{24}H_{24}ClFN_5O_2$ requires 468.160); m. p. 95 – 98 °C. ^{1}H NMR (acetone-d_6, 400 MHz) δ (ppm): 8.55 (s, 1H); 8.50 (d, 1H); 8.24 (dd, 1H); 7.81 – 7.77 (m, 1H); 7.73 (s, 1H); 7.69 (td, 1H); 7.44 (d, 1H); 7.29 (t, 1H); 7.22 (s, 1H); 7.20 (dd, 1H); 4.26 (t, 2H); 3.98 (s, 3H); 3.91 (s, 2H); 2.88 (t, 2H); 2.08 (m, 2H). Anal. calcd. (%) for $C_{24}H_{23}ClFN_5O_2$: C, 61.60; H, 4.95; N, 14.97; Found: C, 61.56; H, 5.02; N, 14.78.

Synthesis of 6-(2-(2-(1H-imidazol-1-yl))ethoxy)-4-(3'-chloro-4'-fluoroanilino)-7-methoxy-quinazoline (L3)

Imidazole (138 mg, 2 mmol), tetrabutyl ammonium bromide (16 mg, 0.05 mmol), sodium hydroxide (240 mg, 6 mmol) were added in acetonitrile (20 mL) and the resulting mixture was heated at 80 °C for 1 h, then 6-(2-(2-bromoethoxy)ethoxy)-4-(3'-chloro-4'-fluoroanilino)-7-methoxy-quinazoline (L'1) (517 mg, 1.21 mmol) was added, and the reaction continued for 4 h. After concentrating and cooling to room temperature, the mixture was poured into water (20 mL) and ethyl acetate (10 mL). After filtering, washing by water and ethyl acetate, white solid precipitation was got as the product (389 mg, 78%). ESI-MS (m/z): 414.113 ([M + H]$^+$, $C_{20}H_{18}ClFN_5O_2$ requires 414.109); m. p. 274 – 279 °C. ^{1}H NMR (DMSO-d_6, 400 MHz) δ (ppm): 9.54 (s, 1H); 8.48 (s, 1H); 8.07 (dd, 1H); 7.78 (s, 1H); 7.75 (s, 1H), 7.73 (m, 1H); 7.42 (t, 1H); 7.30 (s, 1H); 7.20 (s, 1H); 6.92 (s, 1H); 4.49 (t, 2H); 4.39 (t, 2H); 3.94 (s, 3H). Anal. calcd. (%) for $C_{20}H_{17}ClFN_5O_2$: C, 58.05; H, 4.14; N, 16.9; Found: C, 58.04; H, 4.20; N, 16.32.

Synthesis of 6-(2-(3-(1H-imidazol-1-yl))propoxy)-4-(3'-chloro-4'-fluoroanilino)-7-methoxy-quinazoline (L4)

Imidazol (138 mg, 2 mmol), tetrabutyl ammonium bromide (16 mg, 0.05 mmol), sodium hydroxide (240 mg, 6 mmol) were added in acetonitrile (20 ml) and the resulting mixture was heated at 80 °C for 1 h, then added 6-(2-(3-

bromoethoxy)propoxy)-4-(3'-chloro-4'-fluoroanilino)-7-methoxy-quinazoline (L'2) (554.0 mg, 1.21 mmol), the reaction was continued for 4 h. After concentrating and cooling to room temperature, the mixture was poured into water (20 mL) and ethyl acetate (10 mL). A white solid precipitation was got by filter, washed by water and ethyl acetate (362.5 mg, 70%). M. p. 201 – 203 °C. ESI-MS (m/z): 428.128 ([M + H]$^+$, $C_{21}H_{19}ClFN_5O_2$ requires 428.128); ^{1}H NMR (DMSO-d_6, 400 MHz) δ (ppm): 9.51 (s, 1H); 8.50 (s, 1H); 8.10 (dd, 1H); 7.78 (s, 1H); 7.76 (m, 1H); 7.64 (s, 1H); 7.43 (t, 1H); 7.23 (s, 2H); 6.91 (s, 1H); 4.20 (t, 2H); 4.08 (t, 2H); 3.97 (s, 3H); 2.30(m, 2H). ^{13}C NMR (DMSO-d_6, 100.6 MHz) δ (ppm): 156.5, 155.1, 153.2, 148.5, 147.6, 137.8, 129.1, 123.9, 122.7, 119.8, 119.3, 119.2, 117.1, 116.8, 109.2, 107.9, 103.5, 66.2, 56.4, 43.4, 30.6. Anal. calcd. (%) for $C_{21}H_{21}ClFN_5O_3$: C, 56.57; H, 4.75; N, 15.71; Found: C, 56.51; H, 4.61; N, 15.46.

General method for preparation of complexes **1** – **3** (see Scheme 1). Ligand (0.4 mmol) and [(η^6-p-cymene)RuCl$_2$]$_2$ (0.2 mmol) were added to 20 mL methanol and the resulting mixture was heated at 65 °C for 4 h, then ammonium hexafluorophosphate (0.8 mmol) was added, and stirred for 1 h. After removing the solvent on a rotary evaporator till 2 – 3 ml, the residue was purified by column chromatography on silica gel using dichloromethane/methanol (30:1) as eluent to give complex as yellow powder.

Complex 1[PF$_6$]: 164 mg, 47%. ESI-MS (m/z): found 724.1191 ([M – PF$_6$]$^+$ requires 724.1195). ^{1}H NMR (acetone-d_6, 400 MHz) δ (ppm): 9.17(d, 1H), 8.76 (s, 1H), 8.15 (d, 1H), 8.09 (t, 1H), 7.99 (s, 1H), 7.77 (bs, 1H), 7.66 (m, 2H), 7.58 (m, 1H), 7.34 (s, 1H), 6.08 – 5.92 (m, 4H), 3.96 (s, 3H), 4.67 (t, 2H), 4.30 (s, 2H), 3.57 (t, 2H), 2.85 (m, 1H), 2.11 (s, 3H), 1.22 (d, 3H), 1.12 (d, 3H). ^{13}C NMR (DMSO-d_6, 100.6 MHz) δ (ppm): 159.6, 157.5, 155.7, 155.4, 155.0, 152.6, 148.6, 139.9, 125.9, 125.5, 125.1, 123.9, 122.0, 119.7, 117.4, 117.2, 108.5, 105.8, 104.8, 97.1, 85.9, 84.32, 83.38, 82.8, 67.6, 61.0, 56.7, 55.3, 31.1, 22.7, 21.3, 17.9. Anal. calcd. (%) for $C_{33}H_{39}Cl_2F_7N_5O_4PRu$ (M + 2H$_2$O): C, 43.77; H, 4.34; N, 7.73; Found: C, 43.34; H, 4.08; N, 7.34.

Complex 2[PF$_6$]: 159 mg, 45 %. m. p. 158 – 161 °C. ESI-MS (m/z): found 738.1372, ([M – PF$_6$]$^+$ requires 738.1352). ^{1}H NMR (DMSO-d_6, 400 MHz) δ (ppm): 9.07 (d, 1H); 8.68 (s, 1H); 8.06 (t, 2H); 7.96 (s, 1H); 7.74 (m, 1H); 7.69 (d, 1H); 7.62 (t, 1H); 7.52 (s, 1H); 7.25 (s, 1H); 5.97 – 5.86 (m, 4H); 4.41 (m, 4H); 4.28 (td, 2H); 3.84 (s, 3H); 2.63 (m, 1H); 2.20 (m, 2H); 1.95 (s, 3H); 1.12 (d, 3H); 1.07 (d, 3H). ^{13}C NMR (DMSO-d_6, 100.6 MHz) δ (ppm): 159.7, 157.4, 155.7, 155.5, 153.3, 151.8, 149.0, 139.9, 125.8, 125.2, 124.0, 123.9, 122.1, 119.6, 119.5, 119.5, 117.4, 117.2, 108.6, 106.2, 103.4, 96.5, 86.3, 84.74, 82.77, 81.8, 67.4, 61.9, 56.6, 55.2, 31.1, 27.9, 22.5, 21.8, 17.9. Anal. calcd. (%) for $C_{34}H_{45}Cl_2F_7N_5O_6PRu$(M + 4H$_2$O): C, 42.73; H, 4.75; N, 7.33; found: C, 42.56; H, 4.08; N, 7.93.

Complex 3: 173 mg, 60%. m. p. 177 – 179 °C. ESI-MS (*m/z*): found 684.0895 ([M – Cl]$^+$, requires 684.0884). ^{1}H NMR (DMSO-d_6, 400 MHz) δ (ppm): 8.49 (s, 1H); 8.39 (d,1H); 8.25 (d, 1H); 8.16 (m, 1H); 7.94 (s, 1H); 7.41 (m, 2H); 7.17 (d, 1H); 5.85 – 5.63 (m, 4H); 4.59 (t, 2H); 4.53 (t, 2H); 3.93 (s, 3H); 2.83 (m, 1H); 2.09 (s, 3H); 1.19 (d, 3H); 0.96 (d, 3H). ^{13}C NMR (DMSO-d_6, 100.6 MHz) δ (ppm): 156.6, 154.7, 153.3, 147.7, 141.4, 137.4, 130.5, 123.8, 122.7, 122.6, 121.6, 116.9, 109.22, 107.81, 106.9, 106.3, 102.4, 100.6, 100.4, 86.8, 86.1, 86.0, 81.6, 56.5, 47.1, 30.4, 22.3, 22.0, 18.3. Anal. calcd. (%) for $C_{30}H_{33}Cl_3FN_5O_3Ru$ (M + H_2O): C, 49.42; H, 4.42; N, 9.61; found: C, 49.13; H, 4.54; N, 9.62.

General method for preparation of complexes **4** and **5** (see Scheme 1). Ligand (0.4 mmol) and [(η^6-*p*-cymene)Ru(en)Cl][PF$_6$] (0.4 mmol) were added to 20 mL methanol and the resulting mixture was heated at 65 °C for 4 h, then ammonium hexafluorophosphate (0.8 mmol) was added and stirred for 1 h. The product was purified by column chromatography on silica gel using dichloromethane/methanol (25:1) as eluent to give the product as white powder.

Complex 4 [PF$_6$]$_2$: 171.8 mg, 43%. m. p. 123 – 125 °C. ESI-MS (*m/z*): found 822.1742 ([M – 2PF$_6$ + CF$_3$COO]$^+$, requires 822.1732). ^{1}H NMR (DMSO-d_6, 400 MHz) δ (ppm): 8.53 (s, 1H); 8.34 (s, 1H); 8.14 (d, 1H); 7.90 (s, 1H); 7.80 (s, 1H); 7.61 (s, 1H); 7.45 (t, 1H); 7.26 (s, 1H); 7.22 (s, 1H); 6.37 (bs, 4H); 5.64 (s, 4H); 4.59 – 4.47 (m, 4H); 3.98 (s, 3H) ; 2.46 (m, 1H); 2.27 (bs, 2H); 2.07 (s, 3H); 1.87 (bs, 2H); 1.00 (d, 6H). ^{13}C NMR (DMSO-d_6, 100.6 MHz) δ (ppm):156.8, 155.1, 155.0, 152.9, 152.7, 148.0, 146.3, 142.4, 136.9, 130.4, 124.3, 123.1, 123.1, 122.6, 119.4, 119.2, 117.1, 116.9, 109.0, 107.1, 106.5, 103.7, 98.5, 83.6, 83.0, 68.0, 56.6, 47.4, 44.8, 30.3, 22.5, 17.5. Anal. calcd. (%) for $C_{32}H_{51}ClF_{13}N_7O_8P_2Ru$ (M + $6H_2O$): C, 34.71; H, 4.68; N, 8.86; found: C, 34.69; H, 4.03; N, 8.96.

Complex 5 [PF$_6$]$_2$: 162.2 mg, 40%. m. p. 138 – 141 °C. ESI-MS (*m/z*): found 836.1872 ([M – 2PF$_6$ + CF$_3$COO]$^+$, requires 836.1888). ^{1}H NMR (DMSO-d_6, 400 MHz) δ (ppm): 8.72 (s, 1H); 8.25 (s, 1H); 8.02 (dd, 1H); 7.98 (s, 1H); 7.73 – 7.71 (m, 1H); 7.62 (s, 1H); 7.52 (t, 1H); 7.29 (s, 1H); 7.23 (s, 1H); 6.36 (bs, 4H); 5.63 (q, 4H); 4.47 (bs, 2H); 4.27 (t, 2H); 4.20 (t, 2H); 4.02 (s, 3H) ; 2.41 (m, 1H); 2.28 (bs, 2H); 2.10 (s, 3H); 1.89 – 1.87 (bs, 2H); 1.05 (d, 6H). ^{13}C NMR (DMSO-d_6, 100.6 MHz) δ (ppm): 157.8, 156.2, 156.1, 153.7, 151.3, 149.2, 142.0, 135.6, 130.5, 125.9, 124.6, 124.5, 122.3, 119.8, 119.6, 117.5, 117.3, 108.3, 106.4, 104.1, 103.8, 103.8, 98.6, 83.5, 83.1, 66.4, 56.9, 45.2, 44.9, 30.3, 29.8, 22.6, 17.6. Anal. calcd. (%) for $C_{35}H_{51}Cl_5F_{13}N_7O_5P_2Ru$ (M + $3H_2O$ + $2CH_2Cl_2$): C, 33.98; H, 4.16; N, 7.93; found: C, 33.55; H, 3.85; N, 8.34.

X-ray crystallography

The single crystals of complex **4** suitable for X-ray analysis was obtained by slowly diffusion of ethyl ether into the methanol solution at ambient temperature. X-ray diffraction analysis was carried out at 173K on a Rigaku Saturn 724+ diffractometer (Rigaku Corporation, Japan) using graphite monochromated Mo radiation (λ = 0.71073 Å) on a Rigaku Saturn 724 CCD area detector, and the structure analysis was performed using SHELXL (Sheldrick, 2013).

Hydrolysis

The stock solutions of complexes **1 – 5** (2 mM) were prepared in methanol. Then 5 μL of the solution (10 μL for complex **2**) was diluted to 200 μL with deionized water in a quartz cuvette and the UV-Vis spectra was recorded by scanning from 200 – 500 nm at certain time intervals at 37 °C. The wavelengths corresponding to the LMCT band at *ca*. 330 – 336 nm were selected for kinetic study. The time-dependent absorbance were fitted by Origin 8.0 (OriginLab Corporation, US) to give the first order rate constant k, and half reaction time $t_{1/2}$ was calculated by formula as follows:

$$A = C e^{-kt} + A_0$$
$$t_{1/2} = \ln2 / k$$

where A is the absorbance, A_0 and C are constants. The species before and after hydrolysis for 1 h were analysed by LC-MS as described below.

High performance liquid chromatography (HPLC)

A Rheodyne sample injector, an Agilent Eclipse XDB-C18 reversed-phase column (150 × 4.6 mm, 5 μm, USA) and an Agilent 1200 series HPLC system were used to analyse the hydrolytic mixtures of complexes **1 – 5**. The mobile phases were water containing 0.1% TFA (A), and acetonitrile containing 0.1% TFA (B). The gradient was increased from 10% to 80% B during 20 min, with a flow rate of 1 mL/min.

Electrospray ionization mass spectroscopy (ESI-MS)

The positive-ion ESI mass spectra were obtained with an Xevo G2 Q-TOF mass spectrometer (Waters, USA) equipped with a Masslynx 4.1 workstation for data analysis. The spray voltage and the cone voltage were 3.3 kV and 5 V, respectively. The desolvation temperature was 350 °C and the source temperature 373 K. Nitrogen was used as both cone gas and desolvation gas with a flow rate of 50 L/h and 800 L/h, respectively. The spectra were acquired in the range of 300 – 1000 Da.

DNA interaction

Hoechst 33342 (20 μM) and CT DNA (200 μM) were dissolved in Tris-HCl buffer (pH = 7.2) and incubated at ambient temperature for 4 h. Then complex **1** or **3** (0 – 16 mM) were added to this solution to make the final concentrations from 0 to 160 μM. After incubating for 12 h, the resulting mixture was measured on an F-4500 fluorescence spectrophotometer (HITACHI) with excitation wavelength at 370 nm and emission spectra from 400 to 650 nm. Modified Stern-Volmer plot[40] was employed to evaluate the affinity of complexes with DNA. Different F_0/F values recorded at 490 nm with different concentrations of complex **1** or **3** was fitted by Origin 8.0 (OriginLab Corporation, US) and K_{sv} was calculated by equations as follows:

$$F_0/F = 1 + K_{sv}[Q]$$

where F_0 and F are the fluorescence intensities of Hoechst-CT DNA complex recorded before and after adding complex **1** or **3**, respectively. [Q] is the concentration of complex **1** or **3**.

EGFR inhibition assay

Enzyme-linked immunosorbent assay (ELISA) was used to evaluate the inhibition of compounds against the activity of EGFR. Various concentrations of the tested complexes in water containing 1% DMSO were added to 4.37 μL DTT buffer and 0.13 μL 188 ng/μL EGFR, after 5 min at room temperature, 25 μL PTP1B (Tyr66), 0.36 μL ATP and 4.14 μL D_2O were added. The mixture was incubated at 37 °C for 1 h, and 18 μL EDTA was added to stop the reaction. Aliquot (25 μL) of the reaction mixture and 75 μL D_2O were transferred to 96-well streptavidin-coated plate and incubated at 37 °C for 1 h. Then the solution was poured out and the plate was washed three times with 200 μL PBS/T. Then 100 μL primary antibody (P-Tyr-100, 1:1000 in PBS/T with 1.5% BSA) was added and incubated at 37 °C for 1 h. After washing three times with 200 μL PBS/T, 100 μL secondary antibody (IgG (H+L), 1:1000 in PBS/T with 1.5% BSA) was added and incubated at 37 °C for 1 h. After washing three times with 200 μL PBS/T, 100 μL TMB (1 mg/mL TMB : Citric acid-phosphate buffer : 30% H_2O_2 = 100 : 900 : 1) was added. After 15 min, 100 μL of 2 M H_2SO_4 was added and the plate was recorded at 450 nm on the ELISA plate reader (SpectraMax M5 Molecular Devices Corporation).

Anti-proliferation assay

The ruthenium complexes were evaluated for anti-proliferative activity against five human cancer cell lines: cervical cancer (HeLa), non-small-cell lung carcinoma (A549), breast cancer (MCF-7), prostate cancer (PC3), and squamous cell carcinoma (A431). The A431 cells was maintained in F12K and others were in DMEM medium supplemented with 10% FBS, 1% PS at 37 °C with 5% CO_2. Aliquot (100 μL) of each cell line in medium was placed in 96-well plates at the following density, A431 80000/mL, A549 50000/mL, MCF-7 70000/mL, PC-3 50000/mL, HeLa 50000/mL, and incubated in the absence or presence of 100 ng/mL epidermal growth factor (EGF, Sigma, USA) for 24 h. Then the medium was removed and 200 μL fresh medium with complexes of various concentrations were added. After incubated at 37 °C for 48 h, the cells were washed with PBS twice and measured by MTT assay.

Docking analysis

All docking studies and molecular modelling were carried out by Surflex-Dock module of Sybyl X 1.1 program, running on Dual-core Intel(R) E5300 CPU 2.60 GHz, RAM Memory 2 GB under the Windows XP system. The crystal structure of the EGFR-erlotinib complex from PDB (1M17)[41] was used as the leading structure to build the corresponding structures of the complexes with EGFR in this work. All the water molecules in the EGFR-erlotinib crystal was eliminated except H2O10 as it plays an important role for the hydrogen bonds between erlotinib and EGFR.[42] After extracting the erlotinib molecule,

the docking pocket was generated at the ATP binding cleft automatically. Then complexes **1 – 5** (in which **1 – 3** are in the hydrolysed form) were successively docked into the pocket, and the molecular models corresponding to the constringent energy gradient (0.05 kcal/mol) were gained. The docking scores are given as $-\log K_D$, which represent the dissociation constants of the EGFR-inhibitor complexes.

Secondary ion mass spectrometry images

SIMS (secondary ion mass spectrometry) analysis and imaging was conducted using a TOF-SIMS V mass spectrometer (IONTOF GmbH, Munster, Germany). Dual-beam depth profiling strategy was used. A 10 keV argon cluster ion beam (Ar_n^+) was used as a sputter beam, which scanned on a 300×300 μm^2 area across the A549 cell surface. The current of the Ar_n^+ was ~ 2 nA with lead-off time 60 μs. A 30.0 keV Bi_3^+ beam with a 200 pA DC current, 100 ns pulse width and repetition rate 5 kHz was applied as an analysis beam, which scanned on a 100×100 μm^2 area at the centre of the Ar_n^+ crater by 256×256 pixels with the highest resolution of 500 nm. Positive spectra were recorded and calibrated by H^+, CH_3^+ and $C_2H_5^+$. The signal intensities were displayed on a colour scale, which were directly related to the concentration of ions of interest.

Fluorescence microscopy

A549 cells (3×10^5 per well) were plated to laser scanning confocal petri dish and grew in the absence of EGF for 24 h. Then the cells were exposed to each complex at 37 °C for 24 h. The fluorescent dyer Hoechst 33342 (2.5 mg) was dissolved in 1 mL deionised water, and then diluted to 25 μg/mL by medium. After removing the cell culture medium and washing once with PBS, 1 mL 1 μg/mL Hoechst 33342 was added and the cells were incubated at 37 °C for 10 min and washed three times with 1 mL PBS. The cells were maintained by minimal colourless medium. Fluorescence images were obtained by a FV1000-IX81 confocal laser scanning microscope (OLYMPUS), at excitation wavelength of 405 nm and emission wavelength of 425 – 500 nm.

Fluorescence-activated cell sorting (FACS) analysis

A549 cells were seeded in a density of 2×10^5 per well in a 6-well plate and cultured for 24 h, then the cells were exposed to different tested compounds at 37 °C for 24 h. The supernatant was removed, and the cells were washed with PBS and detached by trypsin digestion. After washing again with PBS, the cells were transferred to FACS tubes and centrifuged at 1000 rpm for 3 min. After re-suspension in 0.5 mL binding buffer, the cells were incubated with 5 μL Annexin-V conjugate for 5 min, followed by the addition of 5 μL 7-AAD in the dark prior to the FACS analysis. The FACS assays were performed on a Calibur Flow Cytometer (BD, Franklin Lakes, New Jersey, US), of which the FL2 channel was used to record the intensity of Annexin V-PE staining and FL3 channel for 7-AAD staining. The data were analysed by Sell Quest software (BD, Franklin Lakes, New Jersey, US).

Results and discussion

Synthesis and characterisation

To develop desired 4-anilinoquinazoline ligands for coordinating to {(η^6-p-cymene)Ru^{II}} pharmacophore, 4-(3'-chloro-4'- fluoroanilino)-6-hydroxy-7-methoxyquinazoline was reacted with imidazole or 2-(aminomethyl)pyridine to give ligands L1 – L4, respectively (Scheme 1) following a published method.[38, 43] Then the arene-ruthenium(II) dimer complex [(η^6-p-cymene)RuCl$_2$]$_2$ was reacted with ligands L1 or L2 to produce complexes **1** or **2**, respectively, and [(η^6-p-cymene)Ru(en)Cl][PF$_6$] was reacted with L3 or L4 to produce complexes **4** or **5**, respectively.[30, 44] While complex **3** was produced by reacting [(η^6-p-cymene)RuCl$_2$]$_2$ with L3, as shown in Scheme 1. These target complexes were synthesised with moderate yields and their structures were characterised with ^{1}H, ^{13}C NMR, MS, and elemental analysis. The details are given in the experimental section.

In the 1H NMR spectra of complex **1** – **5**, the resonances between 9.2 and 7.2 ppm are assigned to the aromatic protons of the 4-(3'-chloro-4'-fluoroanilino)-7-methoxy-quinazoline and 2-(aminomethyl)pyridine (10H) or imidazole groups (9H). The three protons of the 7-methoxy group of the quinazoline show typical sharp singlet at 3.9 – 4.0 ppm. The aromatic protons of the p-cymene group show resonances at *ca.* 5.9 ppm for complexes **1** – **2** , and *ca.* 5.6 ppm for complexes **3** – **5**. The coordination to ruthenium shifts the resonances of arene protons to the higher field (5.8 – 6.3 ppm). The proton on the tertiary carbon of the isopropyl group in p-cymene shows a typical quintet at 2.4 – 2.8 ppm.

Complexes **1** – **5** have a derived quinazoline group which is the active site of gefitinib. Meanwhile, they have a half-sandwich ruthenium moiety, which is broadly regarded cytotoxic.[32, 45] A flexible two/three-carbon chain connect the above two fragments. This design enable the two active sites exert their individual effects but have minimal influence to each other.
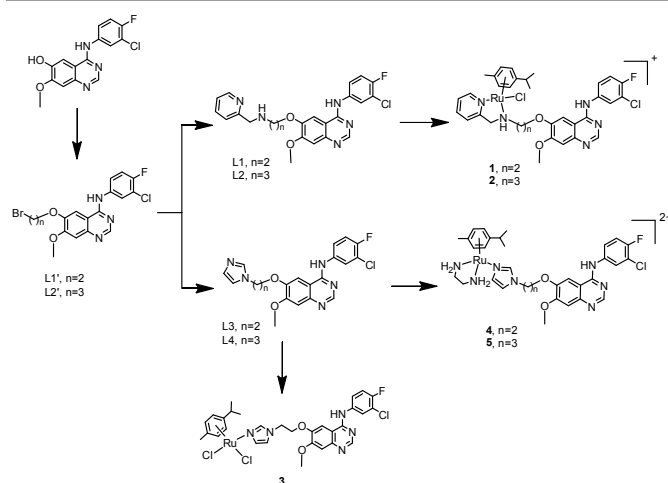
Scheme 1. Synthesis of 4-anilinoquinazoline derivatives L1 – L4 and complexes **1 – 5**.

The structure of complex **4** was further characterised by X-ray crystallography (CCDC deposit number 1061312), as shown in Fig. 1. The structure of complex **4** adopts a triclinic space group. Ru centre forms π coordination bonds with the p-cymene group to construct the typical "piano stool" structure,[12, 15, 32, 46] the rest of coordination sites of Ru occupied by three N atoms (N5, N6, N7) from ethylenediamine and L3. The details of data collection and structure refinement are listed in Table S1 and selected bond lengths (Å), angles and torsions (°) in Table S2 in the supporting information. In solution, two methylene between the quinazoline and the imidazole groups are quite flexible, and distance between the gefitinib activation group and Ru activation group is long enough for both moieties to exert their effects. However, in the EGFR enzyme inhibitory activity experiments below, it was found that the Ru groups in complexes **1**, **2**, **4** and **5** still hinder the binding of the quinazoline unit to the ATP binding pocket of EGFR.
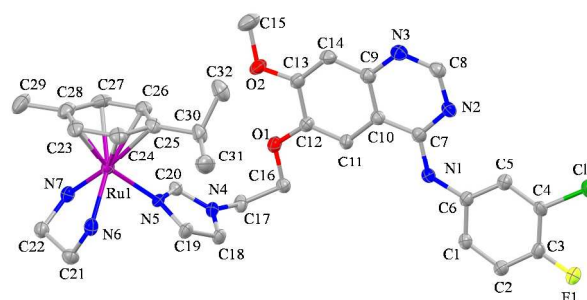
Fig. 1. X-ray crystal structure of the cation of complex **4**. The hydrogen atoms, ethyl acetate, methanol and PF$_6^-$ groups are omitted for clarity.

Hydrolysis of Ru complexes

The hydrolysis of halide leaving groups in {(η^6-arene)Ru^{II}} complexes is broadly considered as an essential step to activate the complexes towards biomolecules.[12, 23] In this work, the hydrolysis reactions of complexes **1** – **5** were carried out in in methanol-water (1 : 40) at 37 °C and were followed by UV-Vis spectrophotometry and characterized by HPLC-ESI-MS before and after hydrolysis for 1 h. The time-dependent UV-Vis spectra of the hydrolysis of **1** – **3** are shown in Fig. 2a, c and e. By comparison, no obvious changes in the absorption spectra of **4** and **5** were observed, and are therefore not shown here. The mono/di-aqua species of **1** – **3** were characterized by HPLC-ESI-MS, as shown in Fig. S1 – S3. The ions m/z at 688.1400, 702.1608, 684.0895 and 648.1098 were observed and corresponded to the hydrolytic species **1**-H$_2$O ([(η^6-p-cymene)RuL1(H$_2$O) – H$_2$O – H]$^+$ requires m/z 688.1434) (Fig. S1), **2**-H$_2$O ([(η^6-p-cymene)RuL2(H$_2$O) – H$_2$O – H]$^+$ requires m/z 702.1591) (Fig. S2), **3**-H$_2$O ([(η^6-p-cymene)RuClL3(H$_2$O) – H$_2$O]$^+$ requires m/z 684.0884) and **3**-2H$_2$O ([(η^6-p-cymene)RuL3(H$_2$O)$_2$ – 2(H$_2$O) – H]$^+$ requires m/z 648.1121) (Fig. S3) respectively.

The plots of the hydrolysis kinetics of **1** – **3** are displayed in Fig. 2b, d and f. The rate constants (k) and half-times ($t_{1/2}$) of **1** – **3** were fitted according to first order reaction kinetics,[45] as shown in Table 1. Notably, complex **3** containing two chloride

ligands undergoes two-step hydrolysis, but the second chloride leaves as soon as the first one hydrolyse. For easy demonstration, the hydrolysis of **3** was treated as a single step first order reaction in calculating the kinetics. Di-aqua species **3**-$2H_2O$ was observed as the major product after hydrolysis for only 1 h, as shown in the LC-MS study in Fig. S3 in the supporting information.

The hydrolysis of complex **3** is the fastest ($t_{1/2}$ = 3.3 min), compared to 34 min for complex **1** and 32 min for complex **2**. The hydrolysis kinetics of complexes **1** and **2** is similar to the complexes of general formula $[Ru(\eta^6\text{-arene})Cl(N\text{-}N)]$,[8, 45] and the pseudo-simultaneous hydrolysis of the two chlorides in **3** has also been reported for Ru arene PTA complex (RAPTA, PTA = 1,3,5-triaza-7-phosphaadamantane).[47] The stability of the EGFR inhibiting group with Ru centre may benefit the dual-targeting feature of these complexes.

DNA interaction

Ruthenium complexes $[(\eta^6\text{-arene})Ru^{II}(en)Cl]PF_6$ might exert their anticancer activities by covalently and non-covalently interaction with DNA.[7, 48] The hydrolysis of leaving groups lead to covalently bound to DNA base, in particular guanine, accompanied by the intercalation of the arene ligands into DNA bases.[23, 25, 46, 49] Moreover, interaction of ruthenium complexes with DNA via groove binding is also a very important mechanism for their anti-proliferation activity.[50] Here, the nucleus staining reagent Hoechst 33342 and CT DNA (calf thymus DNA) were used to study the interaction of complexes **1** and **3** with DNA. Free Hoechst 33342 has weak fluorescence which can be enhanced when it binds to DNA at the minor groove.[40] Thereafter, if other DNA minor groove binder is added, Hoechst 33342 can be competitively replaced, resulting in decreased fluorescence intensity. When complex **1** or **3** (from 0.5 to 160 μM) was added to the solution of Hoechst 33342-CT DNA complex and incubated for 12 h, the fluorescence emission were found to decrease with the increased amount of Ru complex added, as shown in Fig. 3. This result suggests that complex **1** and **3** can bind to the minor groove of CT DNA. The Stern-Volmer constant[40] (K_{sv}, quenching constant) was employed to evaluate the binging affinity of the complexes with DNA and the linear Stern-Volmer plot was shown in Fig. S4 in the supporting information. The K_{sv} values of complexes **1** and **3** are 10.3×10^4 and 4.3×10^4 μM^{-1}, respectively, indicating that the minor groove binding of **1** with CT DNA is stronger than that of **3**.

A DNA replication inhibition experiment was also carried out to examine if the ruthenium complexes bound DNA leads to the inhibition of the replication by polymerase. As shown in Fig. S5, the binding of the ruthenium complex **3** to a Homo Sapiens High Mobility Group Box 1 sequence DNA can substantially inhibit its replication.

These results indicates that complexes can interact with DNA so strongly that the function of DNA can be inhibited. Considering the subcellular distribution of Ru complexes, as shown below, the binding to DNA can be substantial *in vitro*.
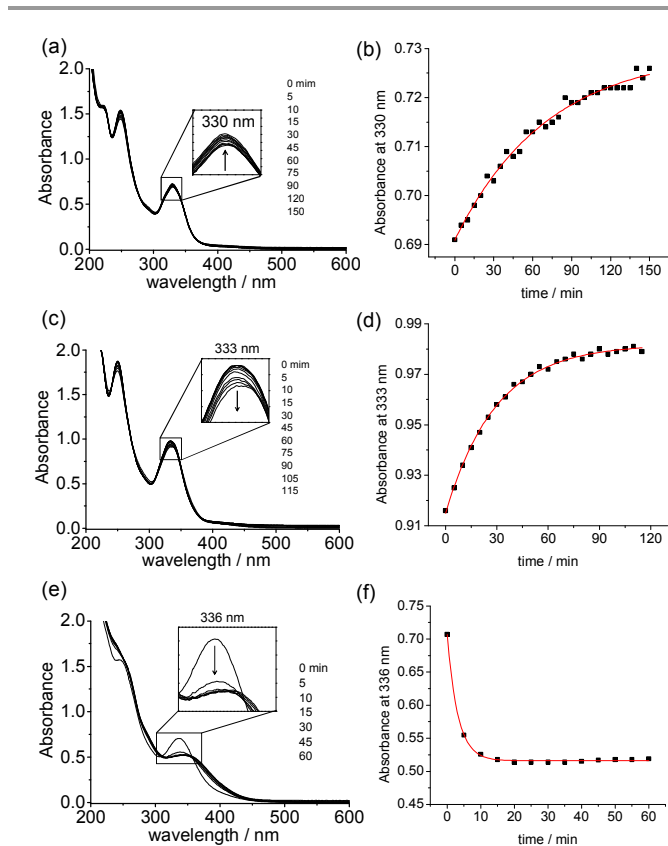

Fig. 2. Time-dependent UV-Vis spectra for the aquation of **1** (a), **2** (c) and **3** (e). The right panel (b, d and f) are the plots of the changes in the absorbance (black square) at selected wavelength (330 nm for **1**, 333 nm for **2** and 336 nm for **3** (aquation of two Cl$^-$), respectively) vs time (squares) and fittings according to first-order reaction kinetics (lines).

Table 1. The hydrolysis rate constants (k) and half-times ($t_{1/2}$) of complexes **1** – **5**.

Complex	**1**	**2**	**3** (1st & 2nd)	**4**	**5**
k (10^{-4} s^{-1})	3.65	3.90	39.7	-[a]	-
$t_{1/2}$ (min)	34.0	32.0	3.3	-	-

[a] No substantial hydrolysis observed.
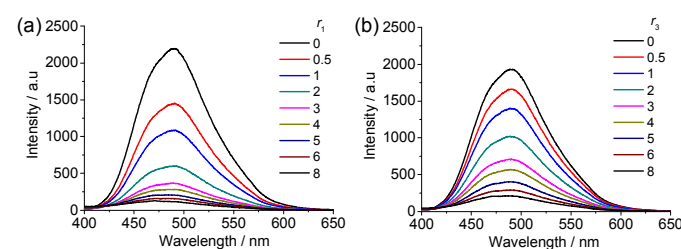
Fig. 3. The fluorescence spectra of Hoechst 33342-CT DNA (20:200 μM) complex reacting with various concentration of complex **1** (a) or **3** (b). The excitation wavelength (λ_{ex}) was 370 nm; r_1 or r_3 is the molar ratio of corresponding complex to Hoechst 33342.

EGFR inhibitory activity

Epidermal growth factor (EGF) stimulates cell growth through binding to its receptor (EGFR) and initiating a series of cellular signal transduction pathways for proliferation and differentiation. Therefore, inhibiting the activity of EGFR

kinase can effectively suppress the EGF stimulated malignance. L3 has been previously shown highly active to inhibit the EGFR activity with half maximal inhibitory concentration (IC_{50}) value of 60.2 nM.[38] Herein, enzyme-linked immunosorbent assay (ELISA) was used to measure the inhibition efficacy of $1 - 5$ towards EGFR with gefitinib as a reference. The IC_{50} values are listed in Table 2 and the dose-dependent inhibition curves shown in Fig. S3 in the supporting information. All of the synthesised complexes are highly active EGFR inhibitors with IC_{50} values at nano-molar level. It should be noticed that for complex **3**, its activity (IC_{50} = 66.1 nM) is very close to its ligand L3, and much higher than the other complexes (**1**, **2**, **4**, and **5**) and even higher than gefitinib (IC_{50} = 94.0 nM). This result suggests that introducing organometallic Ru group can keep the inhibitory activity of the 4-anilinoquinazoline ligands towards EGFR and the existing of the small leaving group, chloride, in this class of complexes may be better than the en group for maintaining their EGFR inhibitory activity.

In vitro anti-proliferation activities

The anti-proliferation activities of complexes $1 - 5$ towards five human cancer cell lines: cervical cancer (HeLa), non-small-cell lung carcinoma (A549), breast cancer (MCF-7), prostate cancer (PC-3), and squamous cell carcinoma (A431) were evaluated. This study was performed either in the presence or in the absence of EGF (100 ng/mL), in order to evaluate the contribution of blocking the signal transduction of EGF to the inhibitory potency of the tested complexes towards the growth of tumour cells. The well-established antitumour drug cisplatin was used as a reference in the absence of EGF, and gefitinib in the presence of EGF. In addition, ruthenium complex RM116[22] was also used as a "(arene)Ru-moiety-only" control against A549 cancer cell line. The IC_{50} values of the tested complexes against each cancer cell line were listed in Table 2.

Complex **1** exhibited least activity among these complexes, showing only low activity against MCF-7 cell line. Complex **2** showed moderate anti-proliferation activity towards A549 cell line in the absence of EGF, and towards A431 cell line in the presence of EGF. Complex **3** and **4** showed high/moderate anti-

proliferation activity towards A549, PC-3, MCF-7 and A431 cell lines in the absence of EGF, and towards A549 and A431 cells in the presence of EGF. Complex **5** showed high/moderate anti-cancer activity towards A549, HeLa, MCF-7 and A431 cell lines in the absence of EGF, and moderate activity against A549 and A431 cell lines in the presence of EGF.

It is usually believed that EGF can cause the conformational change of EGFR, which fully activates the protein kinase and subsequently transduces the signal of cell growth. As a result, a small molecule EGFR inhibitor should become more potent in inhibiting the cell growth when exogenous EGF is added. In this work, as shown in Table 2, only **2** and **3** show EGF dependent anti-proliferation activity against A431 cancer cell line, the IC_{50} values being 53/>100 and 22/32 μM in the presence/absence of EGF. But for the rest of the cases, when EGF was added to the medium, the IC_{50} values are higher than or close to those in the absence of EGF. These results indicate that besides the EGFR inhibition, complexes $1 - 5$ may exert their antitumour activity partially by means of other mechanisms such as DNA interaction as mentioned above, which however may not be efficient enough to counteract the effect of adding EGF.

The overall antitumour activity of complex **3** is higher than **1**, **2**, **4**, **5**. Specifically, in the absence of EGF, the anti-proliferation activity of complex **3** towards A549 cells is even better than RM116, gefitinib or the combined use of RM116 and gefitinib. Moreover, in the presence of EGF, **3** is still comparable to RM116, gefitinib or the combined use of them against the growth of A549 cells. Those results indicate that the possible hydrolysis of two chloride ligands in complex **3** may contribute to the enhanced anticancer activity of this complex. Compared to the previously reported Ru complex [$Ru^{III}Cl_4(DMSO)(L3)$],[38] having the same EGFR inhibiting 4-anilinoquinazoline group (L3), complex **3** has similar potency in inhibiting EGFR, but higher anti-proliferation activity towards MCF-7 cell line in the absence of EGF. More evidence based on the interaction of **3** with EGFR and DNA can be found in docking analysis and mass spectrometry imaging (*vide infra*).

Journal Name

ARTICLE

Table 2. The half maximal inhibitory concentrations (IC_{50}) against A549, HeLa, PC-3, MCF-7 and A431 cell lines (μM), IC_{50} towards EGFR (nM) and *in silico* docking scores (minus logarithm of the disassociation constants) to EGFR ATP binding pocket of complexes **1** – **5** and reference compounds.

	A549 (μM)		HeLa (μM)		PC-3 (μM)		MCF-7 (μM)		A431 (μM)		EGFR (nM)	Docking scores
	+EGF	−EGF	+EGF	−EGF	+EGF	−EGF	+EGF	−EGF	+EGF	−EGF		
1	>100	>100	>100	>100	>100	>100	>100	83 ± 4	>100	>100	180 ± 12	7.1
2	98 ± 3	50 ± 6	>100	>100	>100	>100	>100	88 ± 6	54 ± 7	>100	347 ± 29	6.9
3	31 ± 6	15 ± 2	>100	>100	>100	64 ±9	>100	54 ± 4	22 ± 2	32 ± 7	66 ± 11	8.6
4	52 ± 4	24 ± 4	>100	>100	>100	78 ± 6	>100	73 ± 3	67 ± 6	31 ± 6	145 ± 28	7.4
5	68 ± 6	34 ± 8	>100	48 ± 3	>100	>100	>100	77 ± 4	85 ± 11	29 ± 5	217 ± 14	7.3
gefitinib[a]	20 ± 2	31 ± 3	16 ± 0.5	-[b]	34 ± 3	-	34 ± 2	-	6 ± 1	-	94 ± 3	8.4
cisplatin[a]	-	11 ± 1	-	12 ± 1	-	13 ± 3	-	16 ± 1	-	11 ± 1	-	-
$[Ru^{III}Cl_4(DMSO)(L3)]^{38}$	-	-	-	-	-	-	>100	>100	-	-	60.8 ± 3.5	
RM116[c]	33 ± 4	31 ± 8	-	-	-	-	-	-	-	-	-	-
RM116 + gefitinib	21 ± 2	25 ± 3	-	-	-	-	-	-	-	-	-	-

[a] Cisplatin was used as reference in the absence of EGF, and gefitinib in the presence of EGF

[b] Not tested/applicable.

[c] RM116 = $[(\eta^6\text{-}p\text{-cymene})Ru(en)Cl][PF_6]$

Docking analysis

To further investigate the EGFR inhibiting activity of the newly synthesised ruthenium complexes and 4-anilinoquinazoline derivatives, *in silico* docking analysis was carried out with Surflex-Dock module of Sybyl-X 1.1 program, and the affinity of these compounds with the ATP binding site of EGFR kinase was evaluated. As complexes **1** – **3** are ready to hydrolyse in aqueous solutions, their mono-/di-aqua products were used for docking analysis. The docking scores are given as the minus logarithm of the disassociation constants, as listed in Table 2. The high docking scores of complexes **1** – **5** suggest the high affinity of the small molecules towards EGFR, and the inhibition potency against EGFR given from ELISA is in consistence with the trend (Table 2), indicating the rationality of this docking model. Complex **3** has a docking score of 8.6, which is slightly higher than that of gefitinib (8.4). However, the rest of the complexes are substantially less affinitive towards EGFR than that of gefitinib. We speculate that the bulky organometallic Ru groups in complexes **1**, **2**, **4** and **5** increases the steric hindrance which destabilizes the binding conformation, and therefore reduces their affinity. In contrast, complex **3** has a smaller organometallic Ru group and the Cl ligands may hydrolyse, leading to formation of an additional H-bond between the aqua ligand (H-O-H) and the C=O of Asp831 in EGFR (see Fig. S7a and S7b in the supporting information). This H-bond compromises the steric hindrance and thus increases the affinity of **3** to EGFR.

Subcellular distribution of ruthenium complexes in A549 cells

Inductively Coupled Plasma Mass Spectrometry (ICP-MS) was used to determine the subcellular distribution of the Ru complexes in A549 cells using **3** as an example. The nucleus DNA and membrane proteins were extracted respectively from complex **3** treated A549 cells, and the level of Ruthenium was determined by ICP-MS (experimental details in the supporting information). The Ru was 1058 ± 101 ng per mg membrane protein and 26 ± 11 ng per mg nucleus DNA.

The distribution of Ru in cell level was further determined by secondary ion mass spectrometry (SIMS) to image the presence of ruthenium complexes in single cells. Mass spectrometry images were taken after sputtering with a 10 keV argon cluster ion beam, so the image only shows the existence of Ru inside the cells. Fig. 4 displays the distribution maps
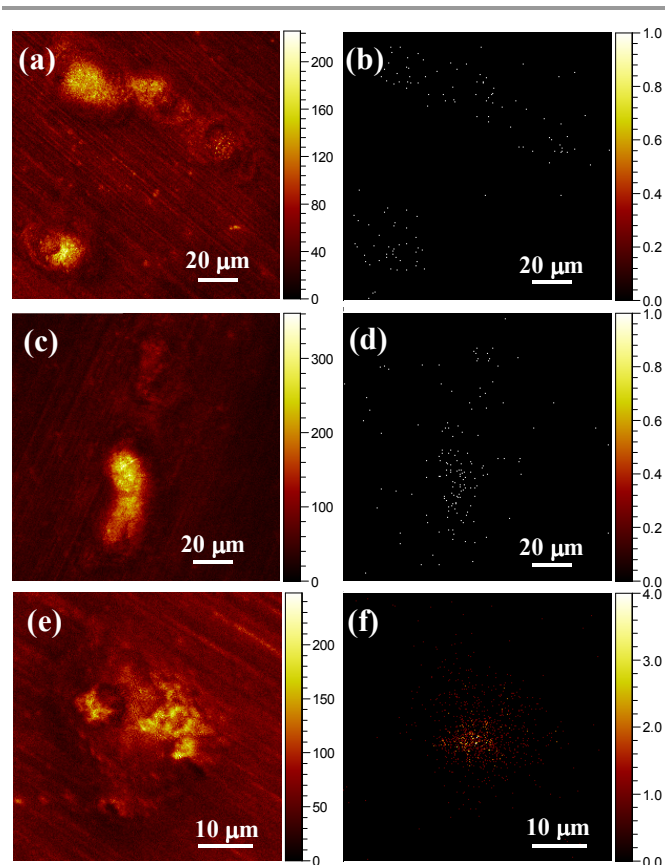
obtained from A549 cells treated with complex **1**, **2** or **3**, respectively. Images of the total ions shown in Fig. 4a, c and e depict the profile of cells; while the images for Ru complexes are shown in Fig. 4b, 4d and 4f. Due to sputtering off of the cell membrane prior to the SIMS imaging, little complexes **1** and **2** were found to localise inside the cells (Fig. 4b and 4d). In contrast, higher level of complex **3** was observed in the central region of the cell (Fig. 4f), which may contribute to the higher anti-proliferation activity of **3** than that of the other complexes.

These results indicates that although a large amount of complex **3** tends to bind to the membrane protein as it has an EGFR binding moiety, it can still enter A549 cell and exert not only enzyme inhibition but also DNA binding effect. This again support the dual-targeting anticancer mechanism of this complex.

Cell apoptosis

As complex **3** is the most cytostatic one against the cancer cell lines among all the metal complexes studied in this work, its mechanism of action was further explored. Fluorescence microscopy imaging was used to evaluate the potential of complex **3**, gefitinib and RM116 to induce apoptosis of A549 cells without additional EGF. The cells were treated with different compounds and were then stained with Hoechst 33342. Their microscopic images are shown in Fig. 5a (blank), 5b (gefitinib), 5c (RM116), 5d (RM116 + gefitinib) and 5e (complex **3**), respectively. Fig. 5b indicates that gefitinib caused the aggregation of the A549 cell nuclei. By contrast, Fig. 5c – e give clear evidence of forming much apoptotic bodies with condensed chromatin, indicating that RM116 and **3** exert their effect by inducing apoptosis

FACS was then used to quantitatively measure the ratio of apoptosis induced by the above compounds (Fig. 5f – j). The results indicated that complex **3** (Fig. 5j) induced a large ratio of A549 cells early-stage apoptosis (56.8%), much higher than those caused by gefitinib (7.52%, Fig. 5g), RM116 (10.7%, Fig. 5h) and combined gefitinib and RM116 (18.6%, Fig. 5i). Gefitinib is regarded as an EGFR inhibitor which mainly blocks the cell signalling pathway initiated by auto-phosphorylation of EGFR and have less capacity to induce apoptosis.[51] In contrast, RM116 containing the cytotoxic organometallic Ru pharmacophore is anticipated to induce more apoptosis.[22] In this work, the coupling of EGFR inhibiting 4-anilinoquinazoline group with $\{(arene)Ru^{II}\}$ moiety in complex **3** produces "1 + 1 > 2" effect in inducing A549 apoptosis, in particular early-stage apoptosis (56.8%). These results suggest the success of developing dual-targeting anticancer complexes based on the synergetic effect of mono-functional pharmacophores.

Fig. 4. SIMS images obtained from A549 cells treated with complex **1** (a and b), **2** (c and d), and **3** (e and f), respectively. The left panel (a, c and e) are total ion images; right panel (b, d and f) are images of ions at m/z 689.7 ([**1** − Cl − H]⁺, calcd. 689.2), 703.8 ([**2** − Cl]⁺, calcd. 703.2), and 649.3 ([**3** − 2Cl − H]⁺, calcd. 649.1), respectively. Fields of view for complexes **1** − **3** are 150 × 150 μm, 150 × 150 μm and 50 × 50 μm, respectively.
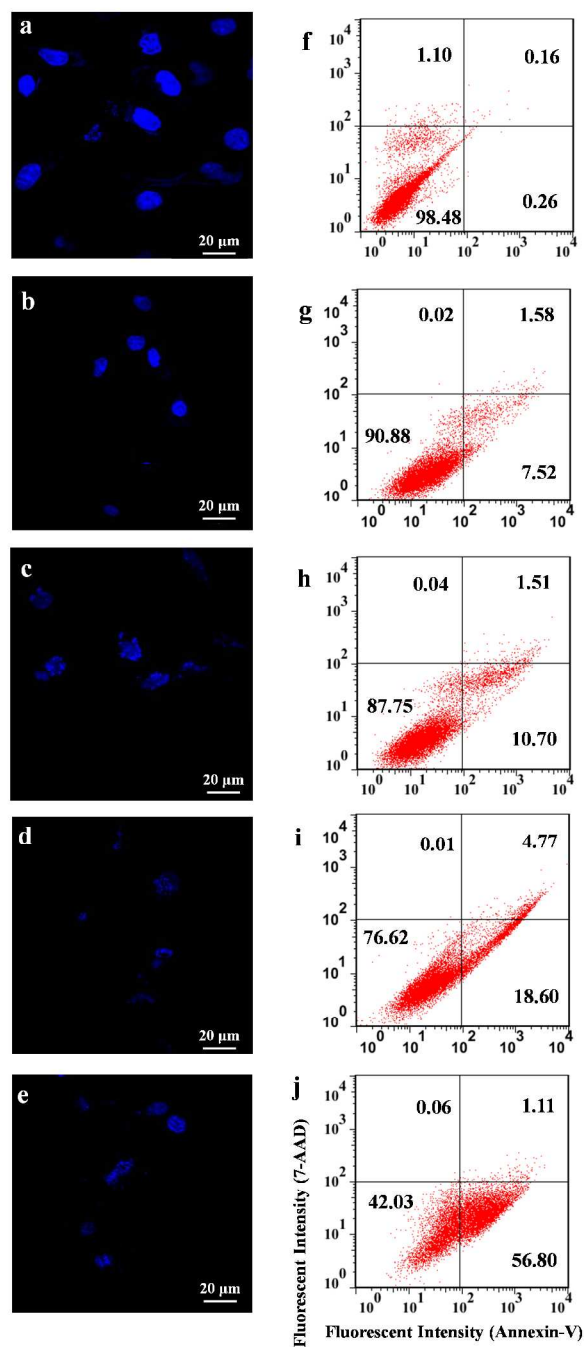
Fig. 5. Confocal fluorescent images (a – e) with emission at 405 nm and flow cytometric quantification (f – j) of viable (bottom left), early-stage apoptotic (bottom right), late-stage apoptotic (top right) and necrotic (top left) A549 cells treated with 50 μM of respective compounds in the absence of EGF at 37 °C for 24 h. The number in each quadrant shows the corresponding percentages of total cell populations. Compounds used: blank (a, f); gefitinib (b, g); RM116 (c, h); RM116 + gefitinib (d, i); complex **3** (e, j).

Conclusions

In summary, a series of organometallic Ru^{II} complexes containing an EGFR inhibiting 4-anilinoquinazoline ligand as potent antitumour agents have been designed and synthesised.

Their structures were characterised and the hydrolysis properties were investigated. These complexes exhibited strong EGFR inhibiting activity and high affinity to DNA via minor groove binding. The in vitro screening results indicated that this group of complexes are moderately active to inhibit the growth of A549 cancer cell line, and the anti-proliferative activity of the most active complex **3** approaches to that of cisplatin, being higher than those of gefitinib, complex [Ru^{III}Cl$_4$(DMSO)(L3)] with similar EGFR inhibiting 4-anilinoquinazoline group, arene ruthenium complex RM116, and combined gefitinib and RM116. Intriguingly, complex **3** was shown to induce much higher level of early stage apoptosis of A549 cancer cell line than gefitinib, RM116, and combined gefitinib and RM116. These findings validate the dual-targeting features of the EGFR-inhibiting and DNA-binding organometallic ruthenium anticancer complexes developed in this work and provide insights into the future development of more effective and specified antitumour agents.

Acknowledgment

Notes and references

1. B. W. Harper, A. M. Krause-Heuer, M. P. Grant, M. Manohar, K. B. Garbutcheon-Singh and J. R. Aldrich-Wright, *Chem. Eur. J.*, 2010, **16**, 7064-7077.
2. C. A. Rabik and M. E. Dolan, *Cancer Treat Rev.*, 2007, **33**, 9-23.
3. Y. W. Jung and S. J. Lippard, *Chem. Rev.*, 2007, **107**, 1387-1407.
4. Y. Fu, M. J. Romero, A. Habtemariam, M. E. Snowden, L. J. Song, G. J. Clarkson, B. Qamar, A. M. Pizarro, P. R. Unwin and P. J. Sadler, *Chem. Sci.*, 2012, **3**, 2485-2494.
5. Z. Liu, A. Habtemariam, A. M. Pizarro, S. A. Fletcher, A. Kisova, O. Vrana, L. Salassa, P. C. A. Bruijnincx, G. J. Clarkson, V. Brabec and P. J. Sadler, *J. Med. Chem.*, 2011, **54**, 3011-3026.
6. E. Meggers, *Curr. Opin. Chem. Biol.*, 2007, **11**, 287-292.
7. P. C. A. Bruijnincx and P. J. Sadler, *Curr. Opin. Chem. Biol.*, 2008, **12**, 197-206.
8. C. G. Hartinger and P. J. Dyson, *Chem. Soc. Rev.*, 2009, **38**, 391-401.
9. G. Gasser, I. Ott and N. Metzler-Nolte, *J. Med. Chem.*, 2010, **54**, 3-25.
10. A. Levina, A. Mitra and P. A. Lay, *Metallomics*, 2009, **1**, 458-470.
11. G. Sava, A. Bergamo and P. J. Dyson, *Dalton Trans.*, 2011, **40**, 9069-9075.
12. F. Y. Wang, A. Habtemariam, E. P. L. van der Geer, R. Fernandez, M. Melchart, R. J. Deeth, R. Aird, S. Guichard, F. P. A. Fabbiani, P. Lozano-Casal, I. D. H. Oswald, D. I. Jodrell, S. Parsons and P. J. Sadler, *Proc. Natl. Acad. Sci. USA*, 2005, **102**, 18269-18274.
13. M. Frasconi, Z. Liu, J. Lei, Y. Wu, E. Strekalova, D. Malin, M. W. Ambrogio, X. Chen, Y. Y. Botros, V. L. Cryns, J.-P. Sauvage and J. F. Stoddart, *J. Am. Chem. Soc.*, 2013, **135**, 11603-11613.
14. T. Kuester, N. Lense, F. Barna, A. Hemphill, M. K. Kindermann, J. W. Heinicke and C. A. Vock, *J. Med. Chem.*, 2012, **55**, 4178-4188.
15. R. E. Morris, R. E. Aird, P. D. Murdoch, H. M. Chen, J. Cummings, N. D. Hughes, S. Parsons, A. Parkin, G. Boyd, D. I. Jodrell and P. J. Sadler, *J. Med. Chem.*, 2001, **44**, 3616-3621.
16. J. K. Barton, A. T. Danishefsky and J. M. Goldberg, *J. Am. Chem. Soc.*, 1984, **106**, 2172-2176.
17. C. Turro, D. B. Hall, W. Chen, H. Zuilhof, J. K. Barton and N. J. Turro, *J. Phys. Chem. A*, 1998, **102**, 5708-5715.

18. B. Cebrian-Losantos, E. Reisner, C. R. Kowol, A. Roller, S. Shova, V. B. Arion and B. K. Keppler, *Inorg. Chem.*, 2008, **47**, 6513-6523.

19. T. W. Hambley, *Dalton Trans.*, 2007, 4929-4937.

20. G. Sava, A. Bergamo, S. Zorzet, B. Gava, C. Casarsa, M. Cocchietto, A. Furlani, V. Scarcia, B. Serli, E. Iengo, E. Alessio and G. Mestroni, *Eur. J. Cancer*, 2002, **38**, 427-435.

21. R. Trondl, P. Heffeter, C. R. Kowol, M. A. Jakupec, W. Berger and B. K. Keppler, *Chem. Sci.*, 2014, **5**, 2925-2932.

22. R. E. Aird, J. Cummings, A. A. Ritchie, M. Muir, R. E. Morris, H. Chen, P. J. Sadler and D. I. Jodrell, *Br. J. Cancer*, 2002, **86**, 1652-1657.

23. H. M. Chen, J. A. Parkinson, R. E. Morris and P. J. Sadler, *J. Am. Chem. Soc.*, 2003, **125**, 173-186.

24. J. E. Debreczeni, A. N. Bullock, G. E. Atilla, D. S. Williams, H. Bregman, S. Knapp and E. Meggers, *Angew. Chem. Int. Ed.*, 2006, **45**, 1580-1585.

25. H. K. Liu, S. J. Berners-Price, F. Y. Wang, J. A. Parkinson, J. J. Xu, J. Bella and P. J. Sadler, *Angew. Chem. Int. Ed.*, 2006, **45**, 8153-8156.

26. R. Pettinari, F. Marchetti, F. Condello, C. Pettinari, G. Lupidi, R. Scopelliti, S. Mukhopadhyay, T. Riedel and P. J. Dyson, *Organomet.*, 2014, **33**, 3709-3715.

27. T. Storr, K. H. Thompson and C. Orvig, *Chem. Soc. Rev.*, 2006, **35**, 534-544.

28. C. S. Allardyce, P. J. Dyson, D. J. Ellis and S. L. Heath, *Chem. Commun.*, 2001, 1396-1397.

29. A. Kurzwernhart, W. Kandioller, C. Bartel, S. Bachler, R. Trondl, G. Muhlgassner, M. A. Jakupec, V. B. Arion, D. Marko, B. K. Keppler and C. G. Hartinger, *Chem. Commun.*, 2012, **48**, 4839-4841.

30. W. Zheng, Q. Luo, Y. Lin, Y. Zhao, X. Wang, Z. Du, X. Hao, Y. Yu, S. Lu, L. Ji, X. Li, L. Yang and F. Wang, *Chem. Commun.*, 2013, **49**, 10224-10226.

31. D. S. Perekalin and A. R. Kudinov, *Coord. Chem. Rev.*, 2014, **276**, 153-173.

32. A. Habtemariam, M. Melchart, R. Fernandez, S. Parsons, I. D. H. Oswald, A. Parkin, F. P. A. Fabbiani, J. E. Davidson, A. Dawson, R. E. Aird, D. I. Jodrell and P. J. Sadler, *J. Med. Chem.*, 2006, **49**, 6858-6868.

33. H. Bregman, D. S. Williams, G. E. Atilla, P. J. Carroll and E. Meggers, *J. Am. Chem. Soc.*, 2004, **126**, 13594-13595.

34. S. V. Sharma, D. W. Bell, J. Settleman and D. A. Haber, *Nat. Rev. Cancer*, 2007, **7**, 169-181.

35. F. Ciardiello and G. Tortora, *Clin. Cancer Res.*, 2001, **7**, 2958-2970.

36. T. J. Lynch, D. W. Bell, R. Sordella, S. Gurubhagavatula, R. A. Okimoto, B. W. Brannigan, P. L. Harris, S. M. Haserlat, J. G. Supko, F. G. Haluska, D. N. Louis, D. C. Christiani, J. Settleman and D. A. Haber, *N. Engl. J. Med.*, 2004, **350**, 2129-2139.

37. J. G. Paez, P. A. Janne, J. C. Lee, S. Tracy, H. Greulich, S. Gabriel, P. Herman, F. J. Kaye, N. Lindeman, T. J. Boggon, K. Naoki, H. Sasaki, Y. Fujii, M. J. Eck, W. R. Sellers, B. E. Johnson and M. Meyerson, *Science*, 2004, **304**, 1497-1500.

38. L. Ji, W. Zheng, Y. Lin, X. Wang, S. Lu, X. Hao, Q. Luo, X. Li, L. Yang and F. Wang, *Eur. J. Med. Chem.*, 2014, **77**, 110-120.

39. W. Han Ang and P. J. Dyson, *Eur. J. Inorg. Chem.*, 2006, **2006**, 4003-4018.

40. T. Sarwar, S. U. Rehman, M. A. Husain, H. M. Ishqi and M. Tabish, *Int. J. Biol. Macromol.*, 2015, **73**, 9-16.

41. J. Stamos, M. X. Sliwkowski and C. Eigenbrot, *J. Biol. Chem.*, 2002, **277**, 46265-46272.

42. J. Nowakowski, C. N. Cronin, D. E. McRee, M. W. Knuth, C. G. Nelson, N. P. Pavletich, J. Rogers, B. C. Sang, D. N. Scheibe, R. V. Swanson and D. A. Thompson, *Structure*, 2002, **10**, 1659-1667.

43. S. Lü, W. Zheng, L. Ji, Q. Luo, X. Hao, X. Li and F. Wang, *Eur. J. Med. Chem.*, 2013, **61**, 84-94.

44. Y. Zhang, W. Zheng, Q. Luo, Y. Zhao, E. Zhang, S. Liu and F. Wang, *Dalton Trans.*, 2015, **44**, 13100-13111.

45. F. Wang, H. M. Chen, S. Parsons, L. D. H. Oswald, J. E. Davidson and P. J. Sadler, *Chem. Eur. J.*, 2003, **9**, 5810-5820.

46. H. Chen, J. A. Parkinson, S. Parsons, R. A. Coxall, R. O. Gould and P. J. Sadler, *J. Am. Chem. Soc.*, 2002, **124**, 3064-3082.

47. C. Scolaro, A. Bergamo, L. Brescacin, R. Delfino, M. Cocchietto, G. Laurenczy, T. J. Geldbach, G. Sava and P. J. Dyson, *J. Med. Chem.*, 2005, **48**, 4161-4171.

48. O. Novakova, J. Kasparkova, V. Bursova, C. Hofr, M. Vojtiskova, H. M. Chen, P. J. Sadler and V. Brabec, *Chem. Biol.*, 2005, **12**, 121-129.

49. H. K. Liu and P. J. Sadler, *Acc. Chem. Res.*, 2011, **44**, 349-359.

50. M. R. Gill and J. A. Thomas, *Chem. Soc. Rev.*, 2012, **41**, 3179-3192.

51. M. Muhsin, J. Graham and P. Kirkpatrick, *Nat. Rev. Drug Discov.*, 2003, **2**, 515-516.